

MODELLING OF ANGLED JET IMPINGEMENT ON LARGE FLAT SURFACES

Adrian Kelsey[1], Richard Bettis[1] and Graham Tickle[2]
[1]Health and Safety Laboratory, Harpur Hill, Buxton, SK17 9JN, UK
[2]AEA Technology plc, Safety and Risk Management, Stokes House, 402 The Quadrant, Birchwood Park, Warrington, Cheshire, WA3 6AT, UK

Releases of gases from pressurised storage can lead to the formation of momentum jets which may impinge on surfaces, or more generally, on the ground. Development of models to include impingement has been limited by a lack of suitable data for non-normal impingement. This paper describes work that was performed to collect data on a small impinging momentum jet. The data was used to examine Computational Fluid Dynamics (CFD) modelling and to extend an existing integral model.

The effects of impingement of single phase momentum jets onto horizontal surfaces on velocity and concentration were measured for different fluid densities and impingement angles. The observed behaviour was between that for normal impingement and three-dimensional wall jets. Concentration decay downstream of the impingement region was faster than that observed for either free or three-dimensional wall jets.

The data was used to examine the predictive capabilities of CFD for modelling impinging jets. Simple empirical correlations suitable for inclusion in integral jet models have been derived based on the observed behaviour. An existing integral jet model has been modified using these correlations, resulting in an improved agreement with the experimental data.

INTRODUCTION

Accidental releases from pressurised storage can lead to the formation of momentum jets. Such releases may take place in congested regions, where impingement on large surfaces can occur, possibly including impingement on the ground. The development of simple jet models, as used in risk analysis, to include the effects of non-normal impingement on subsequent dispersion has been limited by a lack of suitable experimental data. For this reason the reliability of jet impingement models, such as incorporated in EJECT[1] and AEROPLUME[2] is considered, at best, uncertain. The work described in this paper was funded by the Health & Safety Executive's Competition of Ideas Programme. The work involved undertaking a series of experiments to collect data on small scale, single phase impinging momentum jets. These data were used to examine Computational Fluid Dynamics (CFD) modelling as a supplement to experimental studies and to extend an existing integral model, EJECT.

It was decided, due to the lack of available information, that this study should concentrate on the simpler case of characterising single phase (gaseous), rather than two phase (gaseous and liquid) jet impingement. However, generalisation to two phase releases is ultimately of interest for hazard analysis. Since a significant factor in two phase releases is density, due to either material or temperature, it was decided to examine density effects on single phase impinging momentum jets as part of the study.

EXPERIMENTAL STUDIES

Experimental studies were performed to provide data on two significant aspects of angled single phase impinging jet behaviour: the effect of varying the angle at which a momentum jet strikes a surface and how the effects of buoyancy modified this behaviour. In order to simplify the effects of gravity, and because the ground below an accidental release forms a potential surface for impingement, the experimental jets were directed onto an horizontal, plane surface. The releases were performed without any imposed coflow.

RELEASE MATERIALS

Two gases were chosen to give a neutrally buoyant momentum jet and a "dense gas" momentum jet. To allow the momentum jet to be distinguished from air the neutrally buoyant gas nitrogen was used, which has a density less than 4% below that of air. The dense gas used was chlorodifluoromethane (Refrigerant-22, R-22), this has more than three times the density of air.

GEOMETRY

The jets were impinged onto a smooth, horizontal surface. This was a plywood "table" measuring 4 m along the jet axis and 3 m wide. The surface was set on legs 0.5 m above the laboratory floor, allowing access to the underside of the tabletop for instrumentation.

The jet was created by passing gas through a nozzle made from pipe with 8 mm internal diameter, comprising a tube 0.05 m long attached to a standard pipe compression fitting. The nozzle itself was connected to the "straight through" part of a tee-piece, and thence to the gas supply cylinder via a flexible tube. The stem of the tee-piece was used to mount the nozzle on an adjustable framework, which held it rigidly in place during a test, but allowed for alteration in the nozzle angle and location as required. The stem also held a thermocouple which measured the gas temperature $\sim$0.065 m upstream of the exit, Figure 1.

A coordinate system was defined assuming that the jet from the nozzle was symmetrical about the initial axis of the jet and unaffected by gravity or early effects from impingement. Using these assumptions, a "centreline" for the jet was defined as an extension of the central axis of the nozzle in the initial jet direction (parallel to the nozzle walls). This then defined an "impingement point" at the point where the initial centreline intersected the plane of the tabletop. This was used as the reference (zero) coordinate for further measurements.

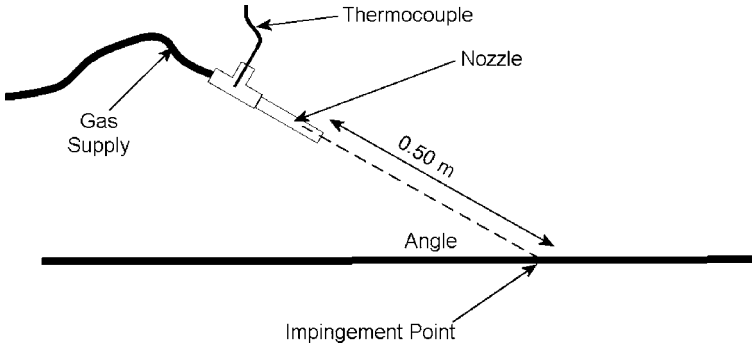

Figure 1. Jet impingement schematic

The impingement angle used was either 30° or 10° from horizontal, with a constant distance of 0.50 m between the exit of the nozzle and the impingement point. The physical impingement point was used for each angle, the change in angle was accomplished by moving the nozzle either upward and forward to give the steeper, 30° angle, or downward and backward for the shallower 10° impingement. The angle and position of the nozzle was checked at intervals during the test programme (typically at the start of a sequence of tests) using an alignment jig.

RELEASE MASS FLOWRATE

A single "target" mass flowrate of 0.01 kg.s^{-1} (10 g.s^{-1}) was used throughout the experimental programme, for both nitrogen and R-22 releases. The denser R-22 releases were thus at a significantly lower velocity and momentum than the nitrogen releases. Using an 8 mm nozzle diameter, flow velocities at the nozzle exit can be calculated, assuming that the pressure is balanced at an ambient pressure of 1 atm. A flow of 0.01 kg.s^{-1} gives exit velocities of $\sim$170 m.s^{-1} for nitrogen and $\sim$55 m.s^{-1} for R-22. This indicates that the flows are subsonic.

The jet mass flow was measured by monitoring the weight of the gas supply cylinder throughout each test release. The cylinder and a support stand were placed on a platform upwind of the release point. The platform used four 250 kg load cells wired in parallel, together with a bridge/amplifier to give a voltage proportional to the platform weight. The individual mass readings were accurate to $\sim$0.1 kg.

MEASUREMENT LOCATIONS

Measurements were made on a grid laid out on the tabletop. Grid points were spaced close together near the impingement point, with increasing spacing for measuring points further away.

Initial tests were performed to assess both the symmetry of the surface jet and the alignment of the jet with the notional centreline. These tests consisted of simple velocity measurements at equal distances to either side of the marked centreline at the furthest part of the surface, where any misalignment or asymmetry would be most marked. These tests showed that there was no measurable difference between velocities on either side of the centreline. Because of this, it was assumed that the jet was, in fact, symmetrical and more detailed measurements could be made by concentrating on only one half of the jet.

The positions on the measurement grid, in the coordinate system based on the notional impingement point are shown in Figure 2.

MEASUREMENT OF GAS CONCENTRATION

The gas concentration was measured using samples taken at the tabletop.

A series of 4 mm diameter holes were made through the surface, and 4 mm OD nylon tubing was inserted into those holes designated for use in a particular run. The

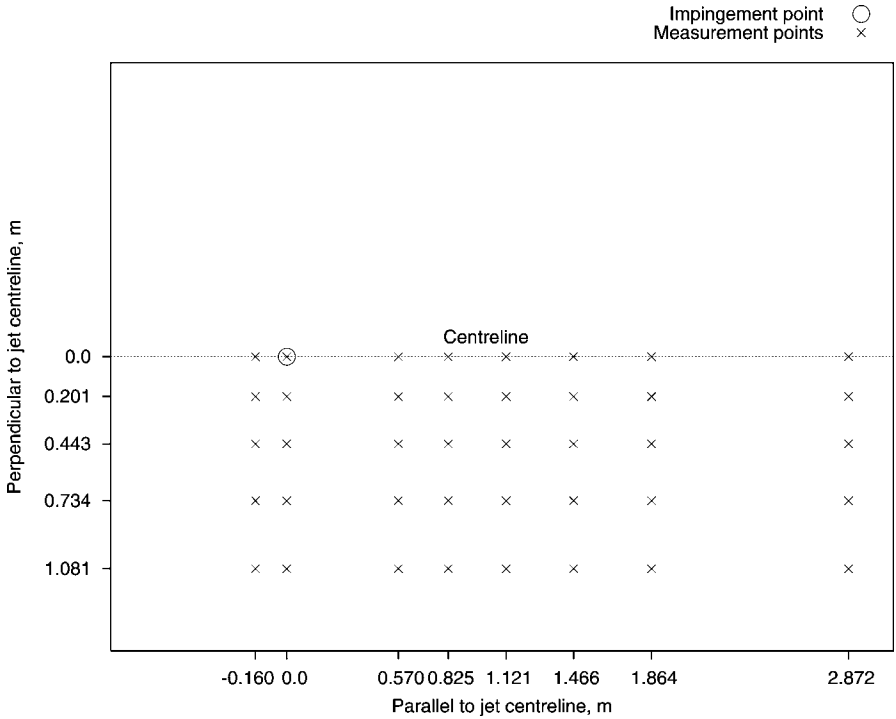

Figure 2. Measurement points

tubing was adjusted so that the end of the tube was flush with the tabletop. Gas was drawn through each tube in turn at a rate of $\sim 1.1\,\mathrm{l\,min^{-1}}$. For most of the test runs an automated system was used to draw gas from each tube in turn, though for some of the later tests the process was duplicated manually.

The gas samples were analysed using a paramagnetic oxygen analyser. This measures the percentage of oxygen in the gas, allowing the level of contaminant gas to be inferred by the reduced oxygen level.

This system has the advantage of using the same equipment for both nitrogen and R-22 jets, reducing the effect that any systematic errors may have on comparing the two. However, as air is normally only 21% oxygen, adding a given percentage of contaminant gas causes a much smaller reduction in oxygen percentage. This effectively reduces the sensitivity of the measurements. The instrument used was able to measure oxygen concentration to an accuracy of 0.05%, so that contaminant concentrations as reported are accurate to $\sim 0.25\%$.

VELOCITY MEASUREMENTS

Initial attempts were made to measure flow velocities in a non-intrusive fashion, using Laser Doppler Anemometry (LDA). However, LDA relies on small particles carried by the flow, and it proved impractical to provide a sufficient level of "seeding" to measure flows at any distance from the nozzle where the jet was well diluted. Consequently, a more direct system had to be used.

The reported velocities were measured with a thermal anemometer probe. The probe was contained in a commercial instrument, housed in a protective sleeve. The sleeve had apertures at either side, allowing air to flow across the heated "needle" that formed the measuring part of the instrument. The presence of the sleeve to either side of the sensor meant that the probe was less sensitive to flows from the "side" than those in the "ideal" direction, passing directly through the aperture. The calibration of the probe is for the direct through flow. It should also be noted that the instrument is not directional, in the sense that it cannot distinguish the direction of the flow it is measuring.

Measurements were made of flow across the surface of the table and vertical profiles along the line of the jet centreline.

CFD SIMULATIONS

All the CFD simulations were performed using CFX-5 from ANSYS-CFX as the solver. The version of the software used was CFX-5.5.1. CFX-5 is a coupled solver, in which all the hydrodynamic equations are solved simultaneously. This gives a robust solver in which solution times scale linearly with mesh size.

DOMAIN

The domain used in the CFD simulations is shown in Figure 3, it was based on the experimental setup. In the CFD simulations the x-z plane was assumed to be a plane of

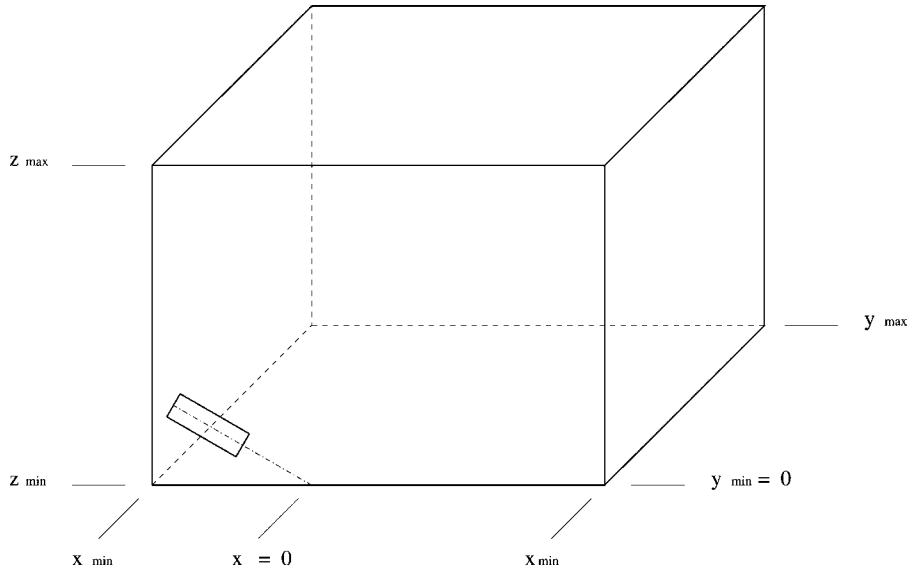

Figure 3. Layout of CFD domain

symmetry halving the size of mesh required. Initial CFD simulations showed possible problems with computational boundaries affecting the predicted flow. Therefore the horizontal dimensions of the CFD domain were increased to 5.5 m long by 5 m wide.

The nozzle exit was represented as an inlet into the domain. A 0.05 m section of nozzle upstream of the exit was represented in the domain to allow the flow to adjust to the presence of the nozzle.

The domain was meshed with an unstructured mesh, simulations were performed at the two experimental nozzle angles. Approximately 300,000 nodes were used for the 10° impingement angle mesh and 550,000 for the 30° impingement angle mesh. In CFX-5 the number of nodes is equal to the number of control volumes used. Other coarser meshes were used when developing an approach to performing the simulations.

CONDITIONS

Simulations were performed of releases in air of the two types of material used experimentally, nitrogen and R-22. The release mass flow rate was kept constant in all the simulations. The release rate used in the CFD simulations was chosen while the experimental releases were still in progress. The value used, 0.008 kg.s^{-1}, was approximately 20% below the average experimental release rates, but within the range of experimental release rates. As with the experimental releases no coflow was imposed.

The release behaviour, and hence the physical modelling necessary, differed with the two materials. The fall in temperature observed during releases was significantly larger during nitrogen releases. Based on the experimental measurements the nitrogen releases were therefore modelled assuming a release temperature of 273 K and including the effects of heat transfer. The R-22 releases were treated as isothermal.

PHYSICAL MODELLING

The flow was always assumed to be turbulent. The CFD simulations used the SST (shear stress transport) turbulence model[3]. Other choices of physical model are shown in Table 1.

The treatment in the near-wall region assumed smooth walls. The near-wall treatment used with the SST turbulence model automatically switched between a wall function approach and a low Reynolds number approach, resolving through to the wall depending on mesh refinement.

NUMERICS

A two stage approach was used to produce the steady state simulation results. In the first stage a 1st order upwind scheme was used for the advection terms. This gave a more stable solution method, at the expense of increased numerical diffusivity. The false timesteps used to improve stability and convergence of the steady state solution were calculated automatically in CFX-5. These calculations were continued until the normalised rms error used in CFX-5 was less than 1×10^{-5} for all variables. In the second stage of the calculations the advection scheme was changed to a 2nd order upwind scheme to reduce errors from use of the 1st order scheme. This 1st order solution was used as the initial condition and the calculations were continued until the normalised rms residuals for the equations were less than 1×10^{-6}.

Each simulation required about 3000 iterations, taking 10 to 14 days on a dual processor 1.7 GHz PC.

RESULTS & ANALYSIS

The experimental results were compared first with the CFD predictions, then with observations published for simpler jet configurations. This shows both the observed and

Table 1. Physical modelling used in CFD simulations

	Nitrogen	R-22
Steady state	Yes	Yes
Flow	Two component gas mixture, ideal gas	Two component gas mixture, ideal gas
Heat transfer	Total energy	Isothermal
Buoyancy	No	Yes

CFD predicted behaviour of angled jet impingement from the current study and how these compare to other simpler cases.

The jet impingement behaviour is taken to be described by the following characteristics:

- decay of maximum velocity and concentration
- growth and vertical and lateral length scales
- any global scaling behaviour, e.g. with release momentum and impingement angle

These characteristics were examined using the maximum velocity, u_m, and the lateral and vertical velocity half widths, $y_{1/2}$, and $z_{1/2}$, these quantities are shown on a schematic velocity profile in Figure 4. Corresponding quantities for concentration, C_m, can also be extracted.

These quantities were non-dimensionalised using the nozzle exit velocity, u_e, and one of two length scales. The velocity related length scales were non-dimensionalised by d_e, defined $d_e = \sqrt{\rho_e/\rho_a}d$ and the concentration (vol/vol) related length scales were non-dimensionalised by d_c, defined $d_c = \sqrt{\rho_a/\rho_e}d$. Where d is the nozzle diameter, ρ_e is the released gas density and ρ_a is the ambient density. The length scales are expected to scale results for different density releases when discharge momentum dominates dispersion. It is convenient to summarise the non-dimensionalised results using simple linear fits to the observed behaviour.

Velocity maximum:

$$\frac{u_e}{u_m} = K_u \frac{x}{d_e} + \frac{u_e}{u_{m,i}}$$

Concentration maximum:

$$\frac{1}{c_m} = K_c \frac{x}{d_c} + \frac{1}{c_{m,i}}$$

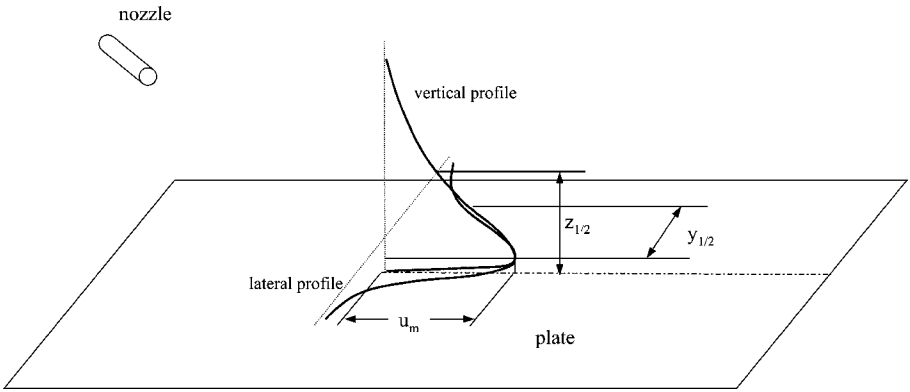

Figure 4. Definition of maximum velocity and vertical and lateral length scales for impinged jet

where K_u and K_c are the slopes of the linear fits to the maximum velocity and concentration data respectively. Subscript i indicates intercept values (at x = 0).

Analogous linear fits can be made for the lateral and vertical spreading.

EXPERIMENT VS CFD

The results of linear fits to the non-dimensionalised data are listed in Table 2, Table 3 and Table 4. Observations from the results are as follows:

1. The maximum velocity and concentration plots were, to a good approximation, linear. This indicates that these quantities decay inversely with distance.
2. The adopted non-dimensionalisation gave a reasonably good collapse between nitrogen and R 22 datasets. This indicates that release momentum dominates dispersion.
3. The experimental data indicated a decay rate of maximum concentration similar to, or slightly more rapid than, the decay of maximum velocity, with ratios of K_c/K_u close to or slightly larger than unity. The CFD predictions indicate significantly less rapid decay for concentration with K_c/K_u close to 0.6 (Table 2).
4. Large lateral spreading was observed. At larger distances significant deviations from linear spread occurred. These spreads are probably subject to the largest measurement uncertainties and have subjectively been omitted from the linear fits given in Table 2 and Table 3.
5. Lateral spread is larger for 30° impingement compared with the 10° case. The CFD predictions of lateral spreading at 30° are also greater than at 10° and are similar to experiments. However, the CFD predictions for lateral spread at 10° impingement are less than observed in the experiments (Table 3).

Table 2. Linear fit parameters to maximum velocity and concentration (vol/vol) decay

		Maximum velocity		Maximum concentration		
Angle (°)	Substance	slope K_u	intercept u_e/u_{mi}	slope K_c	intercept $1/c_{mi}$	Ratio K_c/K_u
			Experiment			
30	Nitrogen	0.22	7	0.27	13	1.22
30	R-22	0.26	−1	0.27	24	1.04
10	Nitrogen	0.20	2	0.20	10	1.01
			CFD			
30	Nitrogen	0.23	5	0.13	13	0.57
30	R-22	0.22	7	0.12	23	0.59
10	Nitrogen	0.12	11	0.077	12	0.64

Table 3. Linear fit parameters for lateral spreading of velocity and concentration (vol/vol)

		Velocity		Concentration		
Angle (°)	Substance	slope β_u	intercept $y_{1/2,i}/d_e$	slope β_c	intercept $y_{1/2,i}/d_e$	Ratio β_c/β_u
			Experiment			
30	Nitrogen	0.44	20	0.59	19	1.34
30	R-22	0.59	8	0.75	21	1.27
10	Nitrogen	0.33	23	0.30	18	0.92
			CFD			
30	Nitrogen	0.62	15	0.73	29	1.18
30	R-22	0.61	8	0.77	49	1.26
10	Nitrogen	0.16	16	0.16	18	0.96

6. The vertical spreading of the jet as indicated by the 30° experimental data is much smaller than the lateral spreading rate. The CFD predictions show a similar vertical spread to the experimental data (Table 4).

ANGLED JET IMPINGEMENT VS SIMPLER JET CONFIGURATIONS

Correlations are published in the literature for the behaviour of jets in simple configurations[4,5,6,7,8,9]. The following jet configurations are considered here:

- Free axisymmetric jet — appropriate when the jet is circular and not interacting with the surface.
- Three-dimensional wall jet — produced when a jet is in contact with and released parallel to the impingement surface.

Table 4. Linear fit parameters for vertical spreading of velocity

		Velocity	
Angle (°)	Substance	slope γ_u	intercept $z_{1/2,i}/d_e$
	Experiment		
30	Nitrogen	0.057	3
	CFD		
30	Nitrogen	0.061	2

- Radial wall jet — produced by an axisymmetric jet impinging at an angle of 90° to the surface.

It should be noted that most of the referenced studies are based on ambient density jets.

Comparing the angled jet impingement behaviour with the simpler geometry behaviour it is found that:

1. The maximum concentration and velocity decay more rapidly for angled impingement compared with both free axisymmetric jets and three-dimensional wall jets (zero impingement angle). However, the velocity decay for angled impingement is less than that for a radial wall jet (90° impingement).
2. The lateral spread is greatly enhanced compared with that of a free jet and is also enhanced above that observed for three-dimensional wall jets (zero impingement angle). The enhancement is most pronounced for the 30° impingement angle, with spreading rates almost six times that of free jets and almost double that of three-dimensional wall jets. For 10° impingement the lateral spreading rate was only about 30% larger than that of a three-dimensional wall jet.
3. The vertical spreading rate at 30° impingement is similar to that for a three-dimensional wall jet (zero impingement angle), and less than that for a radial wall jet (90° impingement), or a free axisymmetric jet.

DEVELOPMENT OF A SIMPLE IMPINGEMENT MODEL FOR INCLUSION IN AN INTEGRAL JET MODEL

EJECT, the HSE/AEA Technology jet dispersion model, already had a simple model of jet impingement[1]. This was based on an abrupt transition to a ground based, three-dimensional, wall jet. Comparison with the experimental data from this project found that the decay of maximum velocity and concentration was too slow, that lateral spreading was too slow and that vertical spreading was overpredicted. A simple model of wall jet behaviour was therefore developed, based on the analysis of experimental data from this work. This simple model is outlined below.

CENTRELINE DECAY

A mass flux, m, may be defined from the momentum flux, J, and the maximum velocity u_m by:

$$m = J/u_m \tag{1}$$

The momentum flux, J, is given by the conditions at the nozzle exit. Assuming uniform profiles at the nozzle exit, the momentum flux is given by:

$$J = \rho_e u_e^2 A_e \tag{2}$$

To describe the dilution of the jet, an empirical entrainment relation of the form

$$\frac{dm}{dx} = E$$

is sought which is consistent with the observed wall jet behaviour.

At large distances from the impingement region, it can be argued on dimensional grounds that the behaviour of the jet depends only on the momentum flux, ambient density and the downstream distance (this is the case so long as there is no ambient flow). One of the simplest entrainment relations consistent with the above is to take

$$E = \alpha \rho_a^{1/2} J^{1/2}$$

where α is an impact angle dependent entrainment coefficient. Since E is constant, this entrainment relation implies

$$m = \alpha \rho_a^{1/2} J^{1/2} (x - x_i) \tag{3}$$

x_i is an offset distance which accounts for the development of the flow from the impingement region to the full developed wall jet.

Substituting for J and m in (3), using (2), and (1) we see that the above entrainment model is directly equivalent to the observed inverse linear decay of velocity with distance:

$$\frac{u_e}{u_m} = K_u \left(\frac{x - x_i}{d_e} \right) \quad \text{with } K_u = \left(2/\sqrt{\pi}\right)\alpha$$

The relation of concentration, c, to the contaminant mass flux m_g, is directly analogous to that of the velocity u to the momentum flux J. Assuming the same profiles for velocity and concentration we obtain:

$$\frac{1}{C_m} = K_c \left(\frac{x - x_i}{d_c} \right) \quad \text{with } K_c = K_u.$$

The experimental data in fact indicate that K_c is slightly larger than K_u, suggesting slightly different velocity and concentration profiles.

LATERAL AND VERTICAL SPREADING

The lateral spreading of the wall jet may be most readily modelled by an equation of the form

$$\frac{dy_{1/2}}{dx} = \beta_u$$

where β_u is the lateral spreading rate which, in the absence of other spreading mechanisms (e.g. gravity induced), depends solely on the impingement angle θ.

Vertical spreading in the model is deduced from mass conservation.

Both centreline decay and lateral spreading depend on impingement angle, θ. An empirical fit to the experimental data for both is given in the next section.

EMPIRICAL FITS FOR IMPINGEMENT ANGLE DEPENDENCE

Fits for the variation in the decay rate of maximum velocity and lateral spreading with impingement angle between 0° and 90° were made using 2nd order polynomials:

$$\frac{\alpha(\theta)}{\alpha(0)} = \frac{K_u(\theta)}{K_u(0)} = 7 \times 10^{-4}\theta^2 + 5 \times 10^{-4}\theta + 1$$

$$\frac{\beta_u(\theta)}{\beta_u(0)} = 8 \times 10^{-4}\theta^2 + 8.8 \times 10^{-3}\theta + 1$$

These used data for three-dimensional wall jets for 0° impingement angle, Davis & Winarto[5] for velocity decay and Launder and Rodi[6] for lateral spreading rate. The linear fits to the experimental observations from this work were used at 10° and 30°. At 90° impingement, data from Rajaratnam[9] was used to give a velocity decay rate and a spreading rate, in the rectangular coordinate system that gives the observed vertical spreading rate. Further data are needed to confirm the adequacy of these fits for impingement angles between 30° and 90°.

A wall jet model with these impingement angle dependencies is included in a revised version of EJECT, giving a fit to the experimental data shown in Figures 5 and 6. It should be noted that these represent tuning to the particular data and should not be viewed as validation against independent data.

CONCLUSIONS

Experimental measurements of the velocity and concentration field in impinging jets have been performed. The measurements were made at two impingement angles to the horizontal, 10° and 30°, using two materials, Nitrogen, neutral buoyancy, and R-22, which has a density greater than three times the density of air.

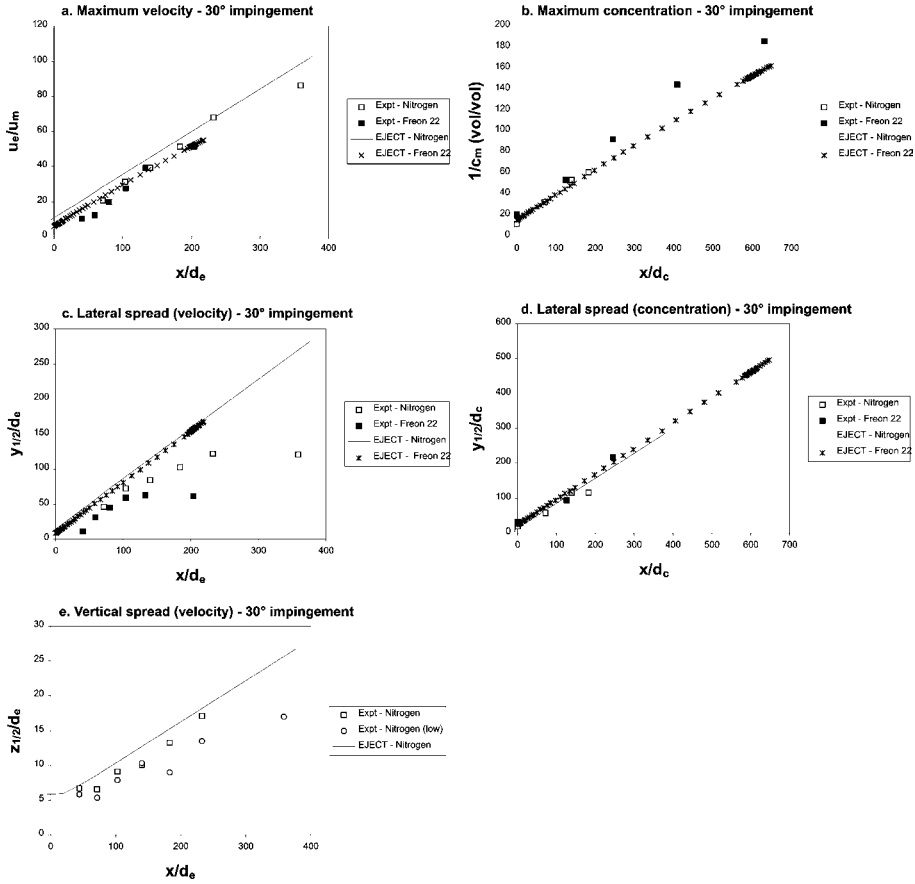

Figure 5. Comparison of predictions using revised EJECT model against experimental data for 30° impingement

The experimental measurements showed that with angled jet impingement there was more rapid decay in maximum concentration and velocity than for axisymmetric free jets and three-dimensional wall jets. Maximum velocity decay is less than for normal impingement. The lateral spreading rate is greater than for either free jets or three-dimensional wall jets. The vertical spreading rate at 30° is similar to a three-dimensional wall jet and less than a free jet.

The experimental data showed that the behaviour downstream of the impingement point can be interpreted as being between that of a wall jet and normal impingement.

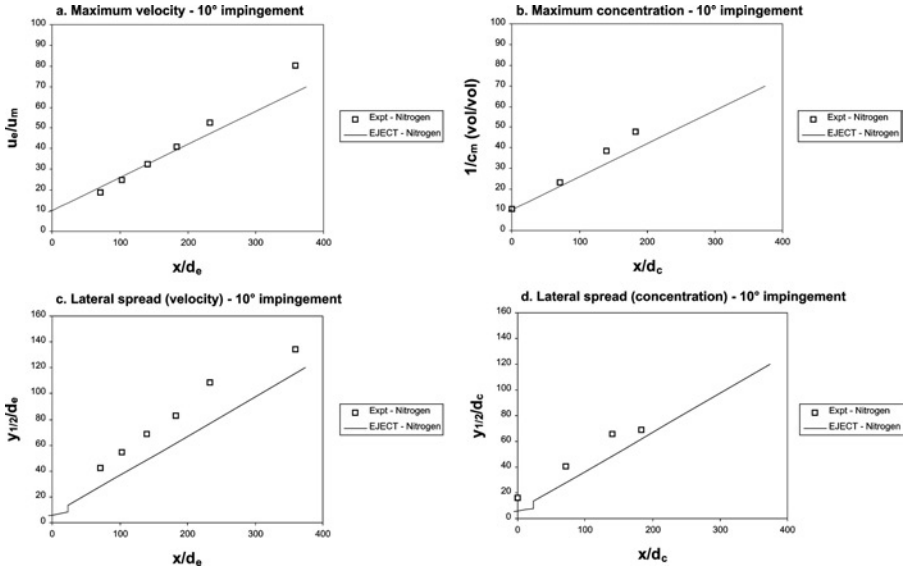

Figure 6. Comparison of predictions using revised EJECT model against experimental data for 10° impingement

The effect of impingement is to reduce the peak downstream concentrations, but to broaden the jet to affect a larger near-field area.

CFD captured qualitative differences in behaviour with varying material and impingement angle. The results of CFD simulations were not used in the development of an integral model of impingement. However, in more complex geometries CFD could, with care in its application, provide useful information on impinging jet behaviour.

A simple wall jet model has been developed that is consistent with experimentally observed wall jet behaviour following angled impingement of single phase momentum jets. The model is based on impingement angle dependent entrainment and lateral spreading rates. The EJECT integral model has been modified using these empirical fits, and shows a good correspondence to the experimental data.

In the scope of this project only limited quantities of experimental data have been collected. This is both in terms of the range of data collected and in cases examined — only single phase jets and only two impingement angles, the greatest of which was only 30° to the horizontal. However, even this limited dataset is useful in showing the influence that angled impingement has on the development of velocity and concentration in the jet. The data have also been shown to be of great value in checking CFD predictions and informing integral model development.

REFERENCES

1. Tickle, G. A., 1998, Extending EJECT to model ground based jets, *AEA Technology Report*, AEAT-2869 Issue 1, July 1998.
2. Post, L. (editor), 1994, HGSYSTEM 3.0 technical reference manual, *Shell Research Ltd*, TNER.94.058.
3. Menter, F., 1994, Two-equation eddy-viscosity turbulence models for engineering applications, *AIAA J*, 23: 1308–1319.
4. Craft, T. J. and Launder, B. E., 1999, The self-similar turbulent three-dimensional wall jet, in *Turbulence and Shear Flow Phenomena – 1*: First International Symposium, Sept 12–15, 1999, Santa Barbara, California, ed. Banerjee, S. and Eaton, J. K., ISBN 1-56700-135-1.
5. Davis, M. R. and Winarto, H., 1980, Jet diffusion from a circular nozzle above a solid plane, *J Fluid Mech*, 101: 201–221.
6. Launder, B. E. and Rodi, W., 1983, The turbulent wall jet – measurements and modelling, *Annu Rev Fluid Mech*, 15: 429–459.
7. Law, A. W.-K. and Herlina, 2002, An experimental study on turbulent circular wall jets, *J Hydraul Eng-ASCE*, 128: 161–174.
8. List, E. J., 1979, Turbulent jets and plumes, in *Mixing in inland coastal waters*, Fischer, H. B., List, J., Koh, C., Imberger, J. and Brooks, N., Academic Press, London, ISBN 0-12-258150-4.
9. Rajaratnam, N., 1976, *Turbulent jets*, Elsevier Scientific Publishing Company, 1976, ISBN 0-444-41372-3.